REPORT DOCUMENTATION PAGE

Form Approved
OMB No. 074-0188

1. AGENCY USE ONLY (Leave blank)	2. REPORT DATE	3. REPORT TYPE AND DATES COVERED
	May 20, 1994	Technical journal, 1994

4. TITLE AND SUBTITLE
CO_2 Non-Local Thermodynamic Equilibrium Radiative Excitation and Infrared Dayglow at 4.3 μm: Application to Spectral Infrared Rocket Experiment Data

5. FUNDING NUMBERS
contract no. F19628-86-C-0118
contract no. F19628-90-C-0060

6. AUTHOR(S)
Henry Nebel, Peter P. Wintersteiner, R.H. Picard, Jeremy R. Winick, and Ramesh D. Sharma

7. PERFORMING ORGANIZATION NAME(S) AND ADDRESS(ES)
Phillips Laboratory
Geophysics Directorate (OPS)
Hanscom Air Force Base, MA

ARCON Corporation
Waltham, MA

8. PERFORMING ORGANIZATION REPORT NUMBER
N/A

9. SPONSORING / MONITORING AGENCY NAME(S) AND ADDRESS(ES)
SERDP
901 North Stuart St. Suite 303
Arlington, VA 22203

10. SPONSORING / MONITORING AGENCY REPORT NUMBER
N/A

11. SUPPLEMENTARY NOTES
Published in *Journal of Geophysical Research*, vol. 99, No. D5, pp. 10409-10419, May 20, 1994. This work was supported in part by contract no. F19628-86-C-0118 & contract no. F19628-90-C-0060.

12a. DISTRIBUTION / AVAILABILITY STATEMENT
Approved for public release: distribution is unlimited

12b. DISTRIBUTION CODE
A

13. ABSTRACT ***(Maximum 200 Words)***

Infrared radiative excitation in non-local thermodynamic equilibrium (non-LTE) regions of the Earth's atmosphere for the ν_3-mode vibrationally excited states of CO_2 under sunlit conditions and the resulting 4.3-μm limb radiance are calculated using a line-by-line (LBL) radiative transfer model. Excited-state population densities and the corresponding vibrational temperature profiles are calculated for the important emitting states using a model which includes radiative absorption and emission as well as various collisional processes. The quenching of $O(^1D)$ by N_2 has a greater impact on these population densities than has been previously reported in literature. Integrated radiance in a limb view for the 4.3 μm bands is calculated from the model and compared with sunlit earthlimb measurements obtained by the Spectral Infrared Rocket Experiment (SPIRE). Solar pumping is the dominant excitation process for the 4.3-μm emitting states in the daytime. This is the first detailed comparison of results of a full line-by-line non-LTE radiative transfer calculation with 4.3-μm earthlimb radiance data.

14. SUBJECT TERMS
infrared radiative excitation, Spectral Infrared Rocket Experiment (SPIRE), SERDP

15. NUMBER OF PAGES
11

16. PRICE CODE
N/A

17. SECURITY CLASSIFICATION OF REPORT	18. SECURITY CLASSIFICATION OF THIS PAGE	19. SECURITY CLASSIFICATION OF ABSTRACT	20. LIMITATION OF ABSTRACT
unclass	unclass	unclass	UL

JOURNAL OF GEOPHYSICAL RESEARCH, VOL. 99, NO. D5, PAGES 10,409–10,419, MAY 20, 1994

CO_2 non-local thermodynamic equilibrium radiative excitation and infrared dayglow at 4.3 μm: Application to Spectral Infrared Rocket Experiment data

Henry Nebel[1]

Phillips Laboratory, Geophysics Directorate (OPS), Hanscom Air Force Base, Massachusetts

Peter P. Wintersteiner

ARCON Corporation, Waltham, Massachusetts

R. H. Picard, Jeremy R. Winick, and Ramesh D. Sharma

Phillips Laboratory, Geophysics Directorate (OPS), Hanscom Air Force Base, Massachusetts

Abstract. Infrared radiative excitation in non-local thermodynamic equilibrium (non-LTE) regions of the Earth's atmosphere for the ν_3-mode vibrationally excited states of CO_2 under sunlit conditions and the resulting 4.3-μm limb radiance are calculated using a line-by-line (LBL) radiative transfer model. Excited-state population densities and the corresponding vibrational temperature profiles are calculated for the important emitting states using a model which includes radiative absorption and emission as well as various collisional processes. The quenching of $O(^1D)$ by N_2 has a greater impact on these population densities than has been previously reported in the literature. Integrated radiance in a limb view for the 4.3-μm bands is calculated from the model and compared with sunlit earthlimb measurements obtained by the Spectral Infrared Rocket Experiment (SPIRE). Solar pumping is the dominant excitation process for the 4.3-μm emitting states in the daytime. The major contribution to the total limb radiance for tangent heights of 55-95 km is made by the fluorescent states at approximately 3600 cm^{-1} which absorb sunlight at 2.7 μm and then emit preferentially at 4.3 μm. The predicted radiance is in good agreement with the SPIRE measurements for all tangent heights in the 50- to 130-km range. This is the first detailed comparison of results of a full line-by-line non-LTE radiative transfer calculation with 4.3-μm earthlimb radiance data.

1. Introduction

In recent years, there has been increasing interest in radiative transfer in the infrared spectral region under non-local thermodynamic equilibrium (non-LTE) conditions in the Earth's atmosphere [e.g., *Kumer*, 1977; *Shved et al.*, 1978; *Kumer and James*, 1982; *Gordiets et al.*, 1982; *Dickinson*, 1984; *Lopez-Puertas et al.*, 1986a,b; *Lopez-Puertas and Taylor*, 1989; *Kutepov et al.*, 1991; *Wintersteiner et al.*, 1992]. These non-equilibrium conditions generally exist in the Earth's mesosphere and thermosphere, where the time between collisions is not much less than the radiative lifetime. Non-LTE infrared emissions play an important role in establishing the global heat balance, structure, and dynamical properties of the middle atmosphere.

In the present paper, 4.3 μm infrared radiation associated with the ν_3 (asymmetric stretch) vibrational mode of CO_2 is considered in the non-LTE region of the quiescent atmosphere under daylit conditions. A future paper will deal with the nighttime emission. A set of codes known collectively as atmospheric radiance code (ARC) is used to calculate (1) the vibrational populations of states that emit at 4.3 μm and (2) the resulting earthlimb radiance. The model calculations are compared to the daytime earthlimb radiance data from the Spectral Infrared Rocket Experiment (SPIRE) [*Stair et al.*, 1985] and it is found that the model results are in excellent agreement with the measurements.

One noteworthy aspect of the ARC codes is that all infrared radiative processes are treated with line-by-line (LBL) algorithms. In particular, the vibrational populations, largely determined by the transfer of radiation within the atmosphere and by the rate of absorption of solar flux, are calculated with the RAD code [*Wintersteiner et al.*, 1992]. The solar flux absorption rates come from a separate LBL code, SABS [*Wintersteiner and Joseph*, 1986], and the earthlimb radiance is subsequently calculated from the level populations with a third code, NLTE [*Wintersteiner and Sharma*, 1985]. This approach has previously been used to model the CO_2 15-μm emission seen by the SPIRE experiment [*Wintersteiner et al.*, 1992].

Comparisons between model calculations and 4.3 μm earthlimb radiance measurements have been carried out previously by *Kumer and James* [1982] using the SPIRE data set and by *Lopez-Puertas and Taylor* [1989] using Stratospheric and Mesospheric Sounder (SAMS) data, but neither of these studies calculated the radiative transfer using a full line-by-line treatment. *Kumer and James* [1982] used a

[1]Now at Alfred University, Alfred, New York.

Paper number 94JD00315.
0148-0227/94/94JD-00315$05.00

band model to calculate the radiative transfer. *Lopez-Puertas and Taylor* [1989] used line-by-line frequency integration to calculate the transmittances of the pressure-modulated cell used in the SAMS experiment, but they used a narrowband model to calculate the radiative transfer. In the present calculation the radiative transfer is calculated by integrating over frequency for each spectral line of a given rovibrational band, using line-specific parameters taken from the HITRAN molecular absorption parameters database [*Rothman et al.*, 1987] for each line. The altitude dependence of the Voigt emission and absorption line shapes as well as the altitude dependence of the line strengths are taken into account for each line in each atmospheric layer. Thus the exchange of photons among layers is calculated very accurately.

Section 2 contains an outline of the model, including the coupling scheme used for the relevant vibrational states, a discussion of the model atmosphere used for the SPIRE simulation, and a description of the SPIRE data set. Section 3.1 contains the results of the calculations for the vibrational temperatures of all the states considered. In section 3.2 the results of the limb radiance calculations are presented and compared with the sunlit portion of the SPIRE data set. Section 4 contains a comparison of the results with those of earlier studies, as well as a discussion of approximations and uncertainties. In section 5 the main points are summarized.

2. Outline of the Model

2.1. Coupling Scheme

The vibrational energy levels of CO_2 used in the present set of calculations are shown in Figure 1. The notation for the levels is that of the HITRAN molecular absorption parameters database [*Rothman et al.*, 1987, 1992], as explained by *McClatchey et al.* [1973]. The ν_3 transitions near 4.3 μm involving emission of one ν_3 quantum are very strong, with Einstein A coefficients ~400 s^{-1}, rather than the ~10 s^{-1} values typical for allowed infrared rovibrational transitions. The lowest-lying 4.3-μm transition is the ν_3 fundamental, 00011-00001. The lowest-lying hot band, 01111-01101, is also important because of the significant probability that the lower state is occupied. Other important 4.3-μm bands originate in higher-lying states having ν_1 and/or ν_2 excitation as well as ν_3 excitation. The states in groups 1 and 2 (see Figure 1) are populated by transitions at 4.3 μm and 2.7 μm, while those in group 3 are populated by 2.0-μm transitions from the ground state. In other words, absorption of solar flux at 2.7 and 2.0 μm is followed, with high probability, by emission at 4.3 μm, and any simulation of daytime conditions must properly account for these solar fluorescent processes [*James and Kumer*, 1973; *Sharma and Wintersteiner*, 1985].

It is important to consider the contributions of three of the minor isotope bands in addition to the bands of the principal $^{12}C^{16}O_2$ isotope. The convention used here, following *McClatchey et al.* [1973], is to designate the major isotope by the digits 626 and the important minor isotopes by 636, 628, and 627 to represent substitutions of ^{13}C, ^{18}O, and ^{17}O, respectively. Table 1 lists all of the bands considered for this study along with some of their important properties. Line parameters for each of the rovibrational transitions have been taken from the 1986 version of the HITRAN database [*Rothman et al.*, 1987].

A coupling mechanism that connects all CO_2 states having ν_3 excitations is the near-resonant V-V process whereby N_2 vibration is exchanged with quanta of asymmetric stretch according to

$$CO_2(v_1v_2v_3) + N_2(v=0) \Leftrightarrow CO_2(v_1v_2v_3\text{-}1) + N_2(v=1), \quad (1)$$

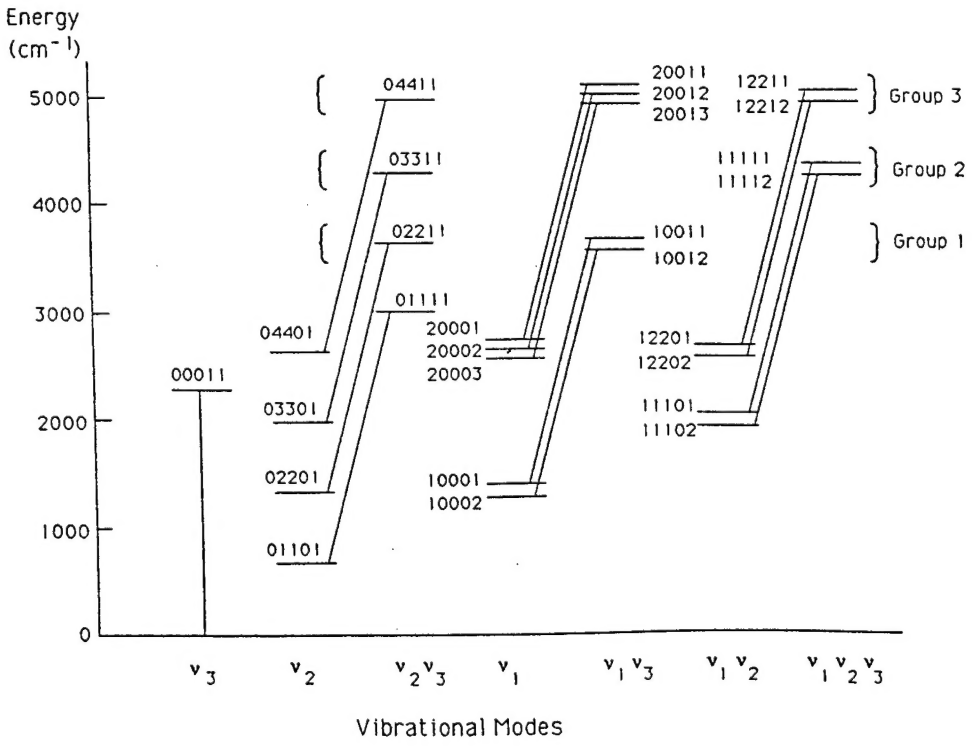

Figure 1. CO_2 vibrational levels and 4.3-μm transitions considered in this study. Absorption at 2.7 and 2.0 μm is not shown.

Table 1. CO_2 Bands Included in the Model for Emission at 4.3 μm

Isotope[a]	Upper State[b]	Lower State[b]	Band Origin cm^{-1}	Transition Wavelength μm	Einstein A Coefficient s^{-1}
626	00011	00001	2349.14	4.26	436.0
	01111	01101	2336.63	4.28	426.3
		Group 1			
	10012	10002	2327.43	4.30	415.4
	02211	02201	2324.14	4.30	418.5
	10011	10001	2326.60	4.30	412.7
		Group 2			
	11112	11102	2315.24	4.32	408.1
	03311	03301	2311.67	4.33	412.5
	11111	11101	2313.77	4.32	404.1
		Group 3			
	20013	20003	2305.26	4.34	398.8
	20012	20002	2306.69	4.34	389.6
	20011	20001	2302.52	4.34	391.6
	04411	04401	2299.21	4.35	402.5
	12212	12202	2302.96	4.34	400.9
	12211	12201	2301.05	4.35	395.5
636	00011	00001	2283.49	4.38	371.5
	01111	01101	2271.76	4.40	368.1
		Group 1			
	10012	10002	2261.91	4.42	364.8
	02211	02201	2260.05	4.42	361.7
	10011	10001	2262.85	4.42	367.2
628	00011	00001	2332.11	4.29	388.2
627	00011	00001	2340.01	4.27	395.7

[a] 626 means $^{16}O^{12}C^{16}C$ and, similarly, for 636, 628, and 627.
[b] Listed in Benedict (HITRAN) notation [*McClatchey et al., 1973*].

where any isotope of CO_2 may be involved. The rate constant for this process was originally calculated by *Sharma and Brau* [1969]. It has been measured for the 626 isotope [*Rosser et al.*, 1969; *Gueguen et al.*, 1975; *Inoue and Tsuchiya*, 1975], and the same value is assumed for the other isotopes. Its value of 5-6 x 10^{-13} cm^3/mol sec at mesospheric and lower thermospheric temperatures is great enough that the process is a determining factor for the vibrational populations of both CO_2 and N_2, which therefore cannot be calculated independently [*Kumer and James*, 1974]. Thus as the first step in these calculations, the 00011 states for the four isotopes 626, 636, 628, and 627 are coupled together along with the $N_2(v=1)$ state. Population densities and vibrational temperatures for these five states are calculated simultaneously using the line-by-line technique of the RAD code, considering as production and loss processes absorption of sunlight and of earthshine (that is, photons originating elsewhere in the atmosphere), spontaneous emission, and the collisional processes 1-10 indicated in Table 2. All absorbed and emitted photons are in the 4.3-μm band. Populations of the group 1 states are taken as known quantities for this calculation: they are used for the determination of the $N_2(v=1)$ vibrational temperature because this state is coupled to the group 1 states as well as to the 00011 states. Coefficients for earthshine absorption are calculated by the RAD algorithm. For the daytime conditions considered here, direct solar pumping at 4.3 μm is accounted for by use of solar flux absorption coefficients from the line-by-line SABS code [*Wintersteiner and Joseph*, 1986]. Rate constants for the collisional interactions are the same as those used by *Lopez-Puertas et al.* [1986b]. The quenching of $O(^1D)$ by N_2 (reaction (7) of Table 2) is assumed to take place with 25% efficiency [*Harris and Adams*, 1983] which means that on average 25% of the energy available from the reaction appears as N_2 vibrational energy. A single collision can produce N_2 with as many as seven vibrational quanta: we assume that multiquantum states quickly relax to an equivalent number of singly excited N_2 molecules.

The non-LTE populations of states of the $CO_2(v_1v_2)$ (bend-stretch) manifold which are used in these calculations are also regarded as known quantities and are assumed to be independent of the state of excitation of states with v_3 quanta which radiate at 4.3 μm. They are calculated by procedures described by *Wintersteiner et al.* [1992], and this assumption is discussed therein. The states of the v_1v_2 manifold include (see Figure 1) the 01101 state having one v_2 quantum, $2v_2$ states with energy near 1335 cm^{-1} (02201, 10001, and 10002), and $3v_2$ states which lie near 2000 cm^{-1} (03301, 11101, and 11102). It is assumed that the $2v_2$ states are in mutual equilibrium, with the same assumption for the $3v_2$ states. The vibrational temperature profiles used here for the

Table 2. Reactions Included in the Model for the $^iCO_2(00011)$, $N_2(1)$, and $^iCO_2(01111)$ Populations

Reaction Number	Reaction[a]	Rate Constant[b] $cm^3/mol\ s$
1	$^iCO_2(00011) + N_2(0) \Leftrightarrow {}^iCO_2(00001) + N_2(1) + 19.2\ cm^{-1}$	$5.0 \times 10^{-13}(300/T)^{1/2}$
2	$^iCO_2(00011) + M \Leftrightarrow {}^iCO_2(03301) + M + 345.9\ cm^{-1}$	$2.22 \times 10^{-15} + 1.22 \times 10^{-10} \exp(-76.75/T^{0.33})$
3	$^iCO_2(00011) + O_2(0) \Leftrightarrow {}^iCO_2(01101) + O_2(1) + 125.4\ cm^{-1}$	$3 \times 10^{-15}\ (1 + 0.02(T - 210))$
4	$^iCO_2(00011) + O \Leftrightarrow {}^iCO_2(03301) + O + 345.9\ cm^{-1}$	$2 \times 10^{-13}\ (T/300)^{1/2}$
5	$N_2(1) + O_2(0) \Leftrightarrow N_2(0) + O_2(1) + 773.5\ cm^{-1}$	$6 \times 10^{-18}\ (T/300)^{1/2}$
6	$N_2(1) + O \Leftrightarrow N_2(0) + O + 2329.3\ cm^{-1}$	$3.2 \times 10^{-15}\ (T/300)^{2.6}$
7	$N_2(0) + O(^1D) \Leftrightarrow N_2(v) + O(^3P)$	2.4×10^{-11}
8	$^1CO_2(10012) + N_2(0) \Leftrightarrow {}^1CO_2(10002) + N_2(1) - 2.5\ cm^{-1}$	$5.0 \times 10^{-13}(300/T)^{1/2}$
9	$^1CO_2(02211) + N_2(0) \Leftrightarrow {}^1CO_2(02201) + N_2(1) - 5.8\ cm^{-1}$	$5.0 \times 10^{-13}(300/T)^{1/2}$
10	$^1CO_2(10011) + N_2(0) \Leftrightarrow {}^1CO_2(10001) + N_2(1) - 3.3\ cm^{-1}$	$5.0 \times 10^{-13}(300/T)^{1/2}$
11	$^iCO_2(01111) + N_2(0) \Leftrightarrow {}^iCO_2(01101) + N_2(1) + 6.7\ cm^{-1}$	$5.0 \times 10^{-13}(300/T)^{1/2}$
12	$^iCO_2(01111) + M \Leftrightarrow {}^iCO_2(04401) + M + 332.3\ cm^{-1}$	$2.22 \times 10^{-15} + 1.22 \times 10^{-10} \exp(-76.75/T^{0.33})$
13	$^iCO_2(01111) + O_2(0) \Leftrightarrow {}^iCO_2(02201) + O_2(1) + 112.5\ cm^{-1}$	$3 \times 10^{-15}\ (1 + 0.02(T - 210))$
14	$^iCO_2(01111) + O \Leftrightarrow {}^iCO_2(04401) + O + 332.3\ cm^{-1}$	$2 \times 10^{-13}\ (T/300)^{1/2}$

[a] The superscript *i* refers to each of the isotopic designations 626, 636, 628, and 627. In reactions (2) and (12), M refers to N_2 and O_2. The exothermicity stated is for reactions involving the major isotope only.

[b] The rate constants are for the reactions in the forward direction and are the same as those used by *Lopez-Puertas et al.* [*1986b*]. T is the kinetic temperature in kelvin.

02201 and 03301 states are similar to those shown in Figure 6 of *Wintersteiner et al.* [1992].

In separate steps, calculations are then performed for the higher-lying states. The 01111 populations are found in a calculation that uses the $CO_2(v_1v_2)$ populations and the previously determined $N_2(v=1)$ population. This procedure is valid because (1) the v_1v_2 manifold populations are quite independent of v_3 excitation, as discussed in the previous paragraph, and (2) the $N_2(v=1)$ population is determined primarily by exchange of vibrational quanta with CO_2 states other than 01111. The radiative transfer in the 01101-01111 band is calculated using the RAD code, considering the collisional processes 11-14 of Table 2. This has been done for the 626 and 636 isotopes, the others being expected to contribute little to the 4.3-μm radiance in the hot band.

The method used to calculate the populations of the higher-lying states of Figure 1 (above 3500 cm^{-1}, groups 1, 2, and 3) under daytime conditions has been described previously [*Sharma and Wintersteiner*, 1985]. These states are very effectively populated in the daytime by the intense short-wave solar flux at 2.7 and 2.0 μm, but relatively little of the energy is reemitted at these wavelengths because of the strong competition from the 4.3-μm emission and, at lower altitudes, the V-V exchange with N_2 (e.g., reactions (8)-(10) of Table 2). Thus the overall short-wave flux is almost entirely solar in origin, as discussed by *Sharma and Wintersteiner* [1985]. Also described in that paper are the collisional interactions among the upper CO_2 states of reactions (8)-(10); these interactions are included in the determination of the populations of those states. A similar statement may be made for the group 2 and group 3 states. Because of the dominance of solar pumping in the excitation of all of these higher-lying states, the calculation neglects the airglow (earthshine) absorption contributions to the populations of these states in the daytime.

2.2. Model Atmosphere for the Spectral Infrared Rocket Experiment (SPIRE) Simulation

To calculate the populations of the 4.3-μm states, a model atmosphere specifying temperature, $[CO_2]$, $[N_2]$, $[O_2]$, [O], and $[O(^1D)]$ as functions of altitude is required. The basic model atmosphere used here is the same as that described by *Wintersteiner et al.* [1992] for application to the 15-μm bands. For temperature and the major constituents the model relies heavily on MSIS 86 [*Hedin*, 1987] above the mesopause and the FASCODE midwinter subarctic atmosphere [*Anderson et al.*, 1986] below the mesopause. The CO_2 mixing ratio profile used here is derived from experimental data and is described as model D by *Wintersteiner et al.* [1992]. Atomic oxygen and CO_2 number densities for this model are shown in Figure 2 of that paper. The $O(^1D)$ number densities are taken from a one-dimensional diurnal photochemical model which was run for the conditions of the sunlit SPIRE data (U. Makhlouf, private communication, 1993).

2.3. SPIRE Data Set

The Spectral Infrared Rocket Experiment (SPIRE) observed the earthlimb in the 1.4- to 16.5-μm spectral region with a

circular variable filter (CVF) spectrometer from the vicinity of Poker Flat, Alaska, at dawn [*Stair et al.*, 1985]. There were 12 spatial limb scans, each consisting of a number of spectral scans, with tangent heights ranging from 0 to 200 km. The payload was exoatmospheric and sunlit. Seven spatial scans looked across the dawn terminator, the eighth looked almost entirely at darkened regions, and for the other four spatial scans the lines-of-sight were entirely sunlit. These three groups of scans are herein referred to as terminator, night, and day scans, respectively. The principal results of the experiment were summarized by *Stair et al.* [1985].

The experimental 4.3-μm radiance, integrated from 4.12 to 4.49 μm, is shown in Figure 2. Scans 1-8 are the terminator and night scans referred to above, where the instrument looked generally toward the west or northwest. Scans 9-12 are the sunlit day scans where the instrument looked generally toward the northeast and east [*Stair et al.*, 1985]. The great disparity between these two data sets emphasizes the important role that solar pumping plays in exciting the CO_2 states that emit at 4.3 μm. For the sunlit scans, the lines-of-sight were illuminated by the Sun over their full extent. Nevertheless, the scans were essentially for "low-Sun" conditions. The solar zenith angle (SZA) varied along each viewing path and varied in a different way for different spatial scans. For those spectral scans with tangent heights near 80 km the SZA at the tangent point varied from 78° to 84° for spatial scans 9-12. Similar variations in SZA occur for other tangent heights (e.g. 77° to 83° for 40 km and 79° to 86° for 120 km). There is no apparent systematic variation in the observed limb radiance in different spatial scans 9-12 for a given tangent height (see Figure 11). These day scans are therefore modeled with a fixed SZA of 78°.

3. Results for the SPIRE Simulation

3.1. Vibrational Temperatures

Vibrational temperatures are presented for both nighttime (no solar excitation) and low-Sun daytime conditions to emphasize the importance of solar excitation processes. In this work, all vibrational temperatures are defined with respect to the ground state, as indicated in equation (1) of *Wintersteiner et al.* [1992]. Figure 3 shows the calculated vibrational temperatures of the CO_2(00011) state for the four isotopes studied here, using the model atmosphere discussed above and assuming no solar excitation. Figure 4 gives the same vibrational temperatures for low-Sun daytime conditions with a solar zenith angle of 78°. Unlike the $CO_2(\nu_2)$ case, where the main (626) isotope may be close to LTE as high as 100 km [*Lopez-Puertas et al.*, 1992], the ν_3 states deviate from LTE near 60 km for nighttime conditions and near 45 km for daytime (sunshine-pumped) conditions. From 60 km to near 100 km (night) and from 45 km to near 110 km (day) the vibrational temperature T_{vib} is greater than the kinetic temperature T, as radiative excitation from sunshine or from upwelling earthshine from the warm stratosphere becomes an important excitation process. Above 100-110 km, T_{vib} falls below T because T_{vib} tends to a radiative equilibrium profile and is thus independent of the local kinetic temperature.

Solar flux absorption in the 4.3-μm bands accounts for the large differences between the daytime results of Figure 4 and the nighttime results shown in Figure 3. It is responsible for most features of the daytime profiles above 60 km. In addition, the impact of $O(^1D)$ on the CO_2 vibrational temperatures is greater than previously reported. Without the quenching of $O(^1D)$ by N_2 the vibrational temperatures shown in Figure 4 would be lower throughout the mesosphere and lower thermosphere, and the curves would not deviate from LTE until 55-60 km. This will be discussed further in section 4.1. The differences between the isotopic vibrational temperatures in the mesosphere are largely due to the fact that the minor isotope bands have smaller opacity than the band of the principal (626) isotope due to much smaller number densities. This means that the solar flux penetrates to lower altitudes in the minor species bands in the daytime and the stratospheric earthshine penetrates more effectively into the mesopause region at night. This results in higher values of T_{vib} for the minor isotope levels. Below 100 km the 00011 vibrational temperatures can be much higher than are shown in Figure 4 if the solar zenith angle (SZA) is smaller. Because of radiative transfer upward from this region, the vibrational temperatures of the 00011 states at higher altitudes (110 km and above) may thus depend on the SZA even though the direct

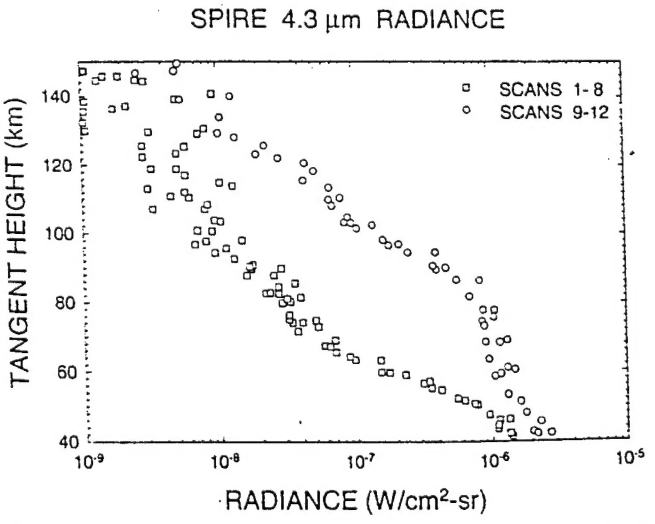

Figure 2. Spectral Infrared Rocket Experiment (SPIRE) limb radiance in the band 4.12-4.49 μm, as a function of tangent height. Terminator and night scans 1-8 are distinguished from sunlit day scans 9-12.

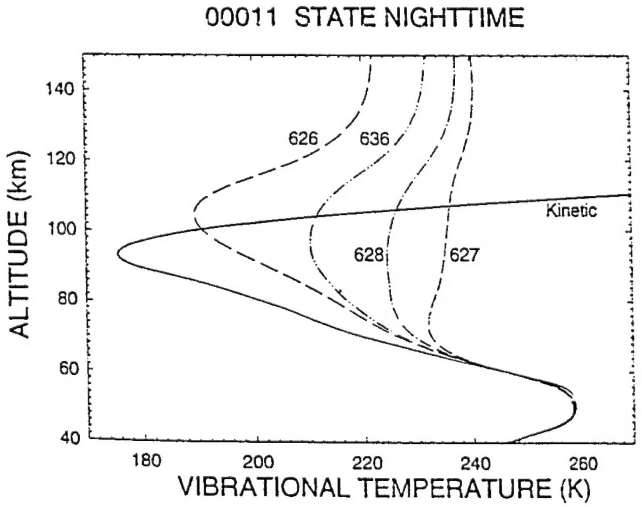

Figure 3. Nighttime vibrational temperatures for the 00011 state for four CO_2 isotopes. The kinetic temperature is also shown for purposes of comparison.

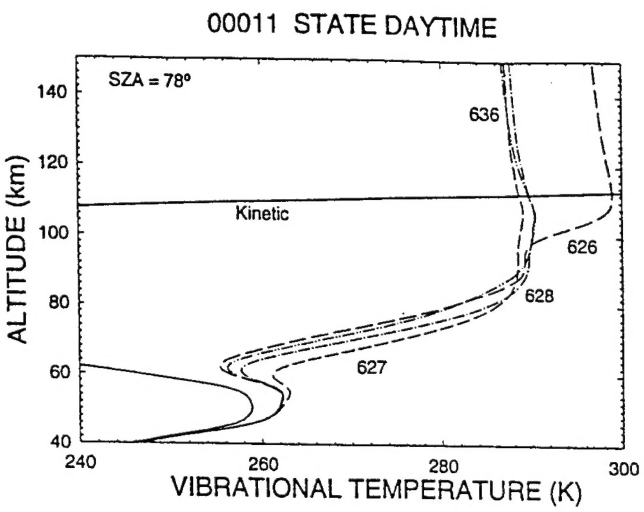

Figure 4. Vibrational temperatures for the 00011 state for four CO_2 isotopes, for daytime conditions with a solar zenith angle of 78°. The kinetic temperature is also shown.

solar excitation rate does not. This point will be discussed further in section 4.1.

Figure 5 shows the N_2 vibrational temperatures from the same calculations that produced Figures 3 and 4, along with the corresponding 626 CO_2(00011) vibrational temperatures. At the lower altitudes the N_2 and CO_2 states are very closely coupled and the N_2 vibrational temperature approaches the CO_2 vibrational temperature for both day and night conditions because of the predominance of the rapid intermolecular V-V process, equation (1). At the higher altitudes, on the other hand, the N_2 vibrational temperature approaches the kinetic temperature at night, due to the importance of the thermal process whereby oxygen atoms directly excite N_2 vibration (Table 2, reaction (6)). The N_2(v=1) lifetime is determined in this region by collisions with atomic oxygen rather than the V-V process, equation (1); thus the N_2 vibrational temperature decouples from the CO_2(00011) vibrational temperature and couples instead to the kinetic temperature at night. Under sunlit conditions the N_2 vibrational temperature also decouples from the CO_2(00011) vibrational temperature at the higher altitudes but in this case is driven considerably above the kinetic temperature because of the direct quenching of $O(^1D)$ by N_2.

The vibrational temperature profiles for the CO_2(01111) state for the 626 and 636 isotopes, for daytime conditions with a solar zenith angle of 78°, are shown in Figure 6. The shape of the curves in the lower mesosphere is similar to that of N_2(v=1), indicating the influence of V-V transfer as an excitation process. At 70 km and higher, radiative processes are the principal factors determining the 01111 temperatures. The differences between the 626 and 636 curves are largely due to the different optical thicknesses of the respective bands: for the 636 isotope there is deeper penetration of solar flux, and a greater fraction of the upwelling radiation reaches the middle mesosphere. In the thermosphere the vibrational temperatures of this level are larger than those of previous calculations (see, for example, *Lopez-Puertas and Taylor* [1989], Figure 5). This is due to increased population of the 01101 level (compared to previous results) which in turn is caused by the greater rate constant for collisions between $CO_2(v_2)$ and atomic oxygen [*Wintersteiner et al.*, 1992].

Figures 7-10 show the vibrational temperatures of the higher-lying groups 1, 2, and 3 states of Figure 1 (~3600-5000 cm^{-1}). The values of T_{vib} for the 02211 and 03311 states fall progressively further below T_{vib} values for the other states in their respective groups as altitude increases above 60 km. This is because they are not effectively pumped by solar flux, and the collisional coupling with the other states which are pumped at 2.7 μm becomes inefficient in the mesosphere and thermosphere.

3.2. Limb Radiance

The daytime scans of the SPIRE experiment were modeled by using the vibrational temperatures shown in Figures 4 and 6-10, calculated for a solar zenith angle of 78°, as input to the line-by-line radiance code NLTE [*Wintersteiner and Sharma*, 1985]. This code calculates integrated radiance in a limb view for each spectral line within a band for selected tangent heights and then sums the results to obtain total band radiance. The calculation must be done for each band and each isotope separately. The results, using all the bands listed in Table 1, are given in Figure 11, along with the data points for the daylit scans 9-12 which are repeated from Figure 2. The nominal instrument noise level of about $4x10^{-9}$ Watt cm^{-2} sr^{-1} for this wavelength region [*Stair et al.*, 1985] has been subtracted from the data values for this figure. The agreement of our model with the data at all altitudes is regarded as validation of the model and confirmation that it properly accounts for the processes that are important for exciting $CO_2(v_3)$ states in the daytime.

Figure 12 gives the breakdown of the daytime model radiance into contributions from individual bands or groups of bands. Several features are noteworthy: (1) The strong 626 fundamental 00011-00001 band is responsible for virtually all of the radiance above 110 km. (2) The 626 fundamental plays a relatively unimportant role for limb paths through the mesosphere (55-85 km) where the strong band has become self-absorbed. (3) The major contribution to the total limb radiance for tangent heights of 55-95 km is made by the group 1 fluorescent states lying near 3500 cm^{-1} (see Figure 1),

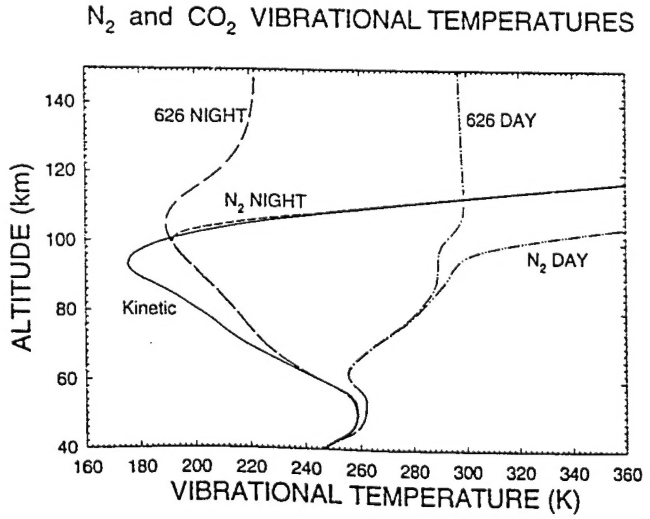

Figure 5. N_2 vibrational temperatures for nighttime conditions and for daytime conditions with a solar zenith angle of 78°. The kinetic temperature is shown for purposes of comparison, as are the night and day CO_2(00011) vibrational temperatures for the 626 isotope.

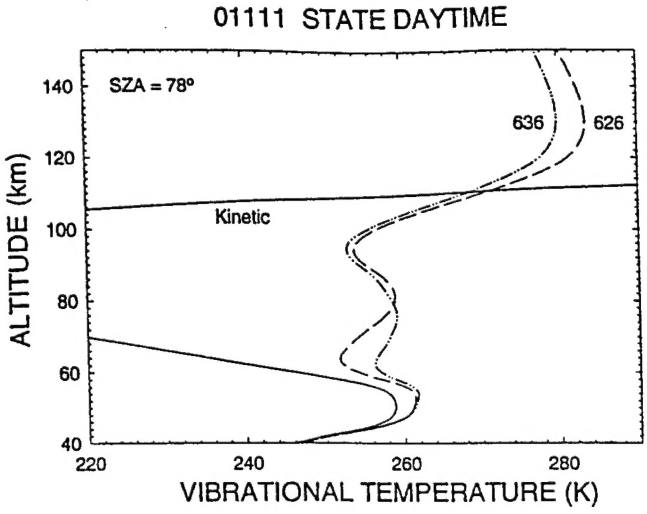

Figure 6. CO_2(01111) vibrational temperatures for daytime conditions with a solar zenith angle of 78°. The kinetic temperature is included for purposes of comparison.

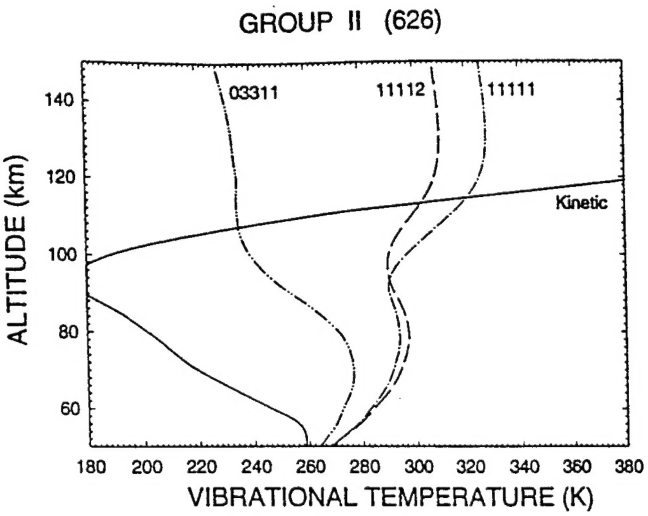

Figure 8. Vibrational temperatures of the group 2 states 11112, 11111, and 03311 of the 626 isotope for daytime conditions with a solar zenith angle of 78°.

particularly the 10011-10001 and 10012-10002 bands, which for the 80-km tangent path account for 60% of the observed limb radiance. Below 80 km the radiance contribution from the group 1 bands falls off as they become self-absorbed. (4) For lower tangent heights near 50 km the contributions from all the groups of bands are roughly comparable, reflecting the differing optical thicknesses of the various bands. The dominance of the fluorescent states from 55 to 95 km and the relative unimportance of the 626 fundamental compared even to the minor isotope fundamentals in the mesosphere were predicted by *Kumer* [1977] based on a band model. Similar conclusions were reached by *Lopez-Puertas and Taylor* [1989] from SAMS measurements. The present work has reached these conclusions using a full line-by-line treatment and is validated by good agreement with the SPIRE data set.

4. Discussion

4.1. Comparison With Previous Studies

The limb radiance profiles obtained here for the different bands (see Figure 12) are similar in general appearance to those calculated by *Kumer and James* [1982], but there are differences in the details. The present calculations predict a lower limb radiance in the vicinity of 80 km for scans having comparable solar elevation and a more rapid drop-off with increasing tangent altitude above 80 km. Some of this results from substantially smaller contributions from the 01111 bands and the minor isotope fundamentals (collectively, the "weak" bands in their report) which occur throughout the range of tangent heights and is most likely due to the great improvement in the treatment of radiative transfer in these bands. The present model also predicts smaller contributions from the 626 fundamental for tangent heights below 75 km, which is probably because the line-by-line approach enables a very careful treatment of the Voigt wings of this extremely opaque band. However, we include bands originating in group 2 and group 3 which contribute below 75 km; these are not in the earlier model, and they partially compensate for the discrepancies in the other bands noted above.

Lopez-Puertas and Taylor [1989], in analyzing SAMS data, also found that emission in hot bands dominates the limb

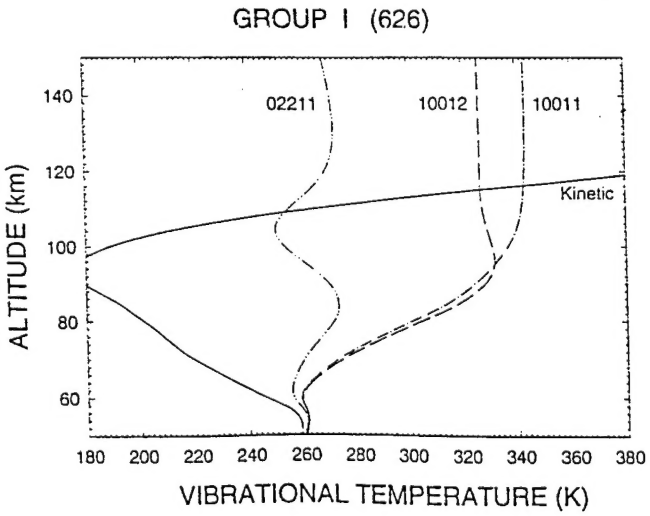

Figure 7. Vibrational temperatures of the group 1 states 10012, 10011, and 02211 of the 626 isotope for daytime conditions with a solar zenith angle of 78°.

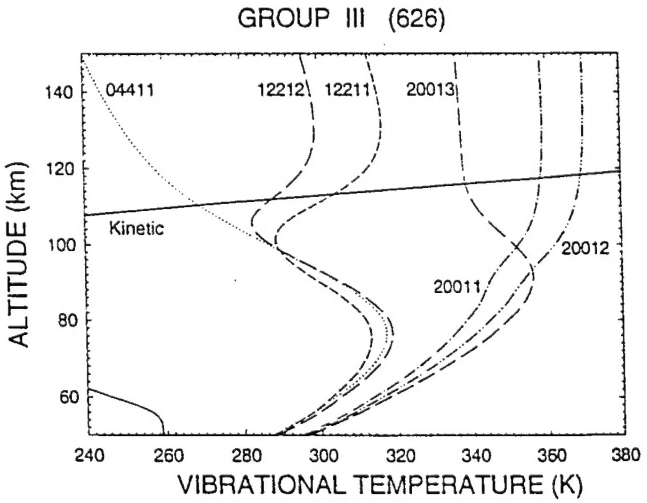

Figure 9. Vibrational temperatures of the group 3 states 20013, 20012, 20011, 12212, 12211, and 04411 of the 626 isotope for daytime conditions with a solar zenith angle of 78°.

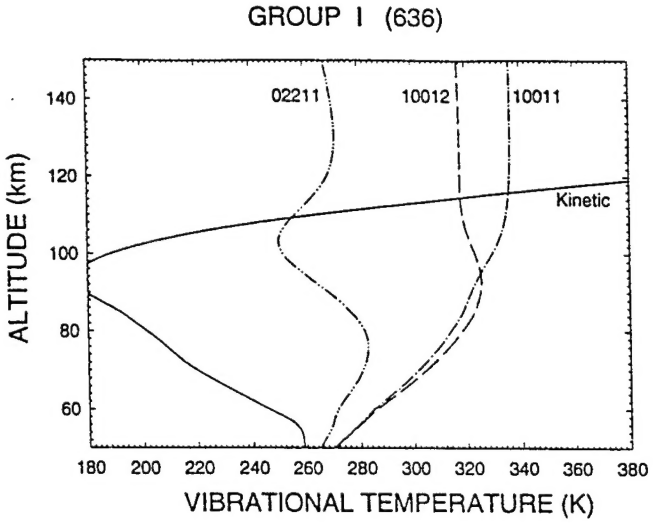

Figure 10. Vibrational temperatures of the group 1 states as in Figure 7, but for the 636 isotope.

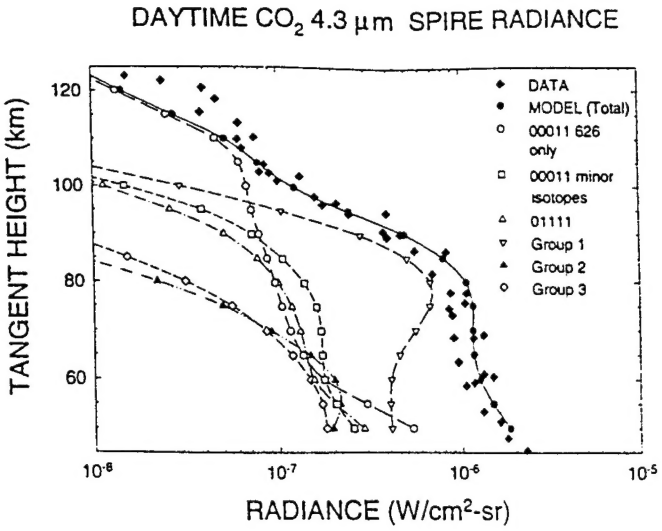

Figure 12. Breakdown of the daytime model radiance into contributions from individual bands or groups of bands. Radiance from the 01111 band and the group 1 bands include contributions from the 626 and 636 isotopes. Radiance from the group 2 and group 3 bands include contributions from the 626 isotope only.

radiance in the mesopause region, but a direct comparison with the present study is frustrated by the fact that the SAMS instrument uses the pressure modulation technique which makes it much more sensitive to the stronger bands. In addition, for the 70°-50°N latitude range, they include the 01111-01101 bands and the group 1 bands in a single profile, making the determination of relative contributions from these bands impossible. For lower latitudes they do find that the group 1 bands give a larger contribution than the 01111-01101 bands in the mesopause region, but the fundamental bands are also important in this region in their study. They also use a different temperature profile which further complicates a direct comparison with the present study.

As mentioned earlier, the quenching of $O(^1D)$ by N_2 has a greater impact on the CO_2 vibrational temperatures than that reported previously by other authors. *Kumer* [1977] considered this process and obtained a maximum enhancement of the $CO_2(00011)$ vibrational temperature of ~4 K at 62 km, using a solar zenith angle of 60°. We find an enhancement of ~5 K for the major 626 isotope due to this process at the same altitude, at a solar zenith angle of 78°. *Harris and Adams* [1983] found that the $CO_2(00011)$ concentration is essentially unaffected by the addition of $O(^1D)$, and *Lopez-Puertas et al.* [1986b] reported that the $CO_2(00011)$ population is not significantly perturbed by the quenching of $O(^1D)$ by N_2, at least for overhead Sun conditions. In contrast, we find that the $CO_2(00011)$ vibrational temperature is enhanced by 4-6 K due to this process throughout the mesosphere, with comparable enhancements in the lower thermosphere.

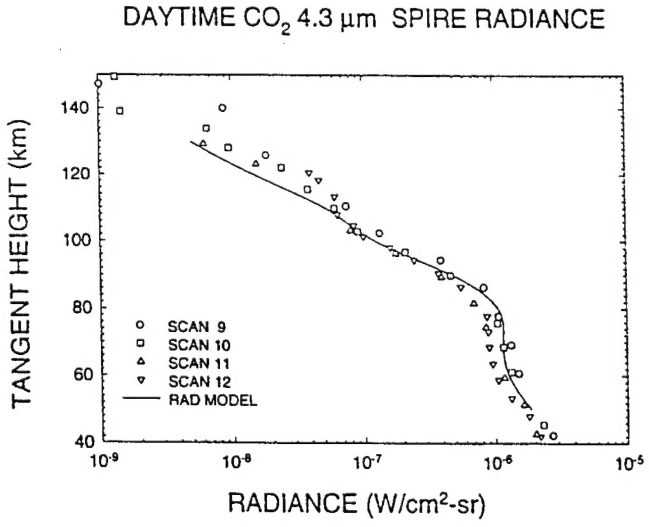

Figure 11. Comparison of the SPIRE limb radiance in the band 4.12-4.49 μm with the daytime model calculation. Data from sunlit scans 9-12 only are plotted.

As indicated in Figure 5, the vibrational temperature of the 626 fundamental is about 298 K in the thermosphere above 110 km. Previous calculations have yielded values between 300 and 310 K [*Kumer*, 1977; *Shved et al.*, 1978; *Lopez-Puertas et al.*, 1986b; *Lopez-Puertas and Taylor*, 1989]. The reason for this difference is that all of the previous calculations were done for a higher Sun than is used in the present set of calculations. When the Sun is higher, the $CO_2(00011)$ state will be populated above 110 km not only by direct solar excitation but also by an increased amount of upwelling radiation (earthshine) from lower altitudes. The latter is due to emission from molecules excited by sunlight that penetrates more deeply into the atmosphere than it does for the low Sun angle considered in the present study. Thus earthshine from below is relatively more important for a high Sun than it is for a low Sun in determining the vibrational temperature of the $CO_2(00011)$ state in the thermosphere. This is indicated in Figure 13 which shows the 626(00011) and $N_2(v=1)$ vibrational temperatures for solar zenith angles of 0°, 55°, and 78°. These curves have been generated using a single profile for $O(^1D)$ (appropriate for a solar zenith angle of 78°) because the purpose of the curves is to compare the importance of upwelling radiation from below on the $CO_2(00011)$ vibrational temperatures in the thermosphere for different solar zenith angles. Note the large variation in the CO_2 curves in the 80- to 110-km region due to the deeper penetration of sunlight for the lower solar zenith angles (higher Sun).

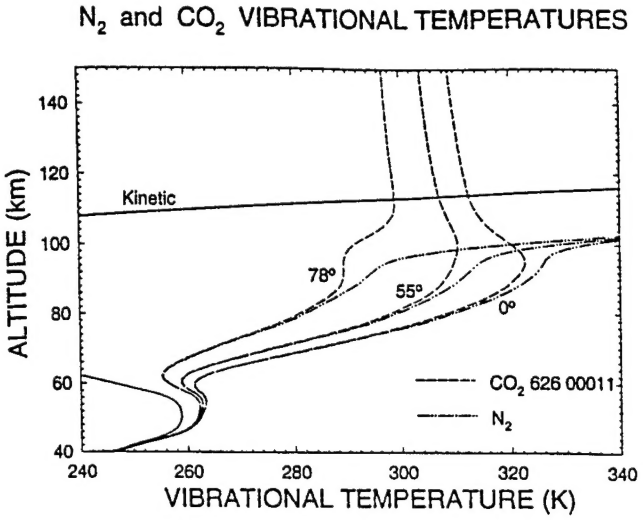

Figure 13. Vibrational temperatures of the N_2(v=1) state and the 00011 state of CO_2 (626 isotope) for solar zenith angles of 0°, 55°, and 78°.

4.2. Approximations and Uncertainties

Several approximations and uncertainties which are inherent in the present set of calculations are now discussed. First of all, there are factors related to the precision of the calculations themselves. Questions of convergence, line overlap, layering, and choice of the lower boundary for the RAD algorithm have been discussed previously [*Wintersteiner et al.*, 1992]. As argued there, any inaccuracies resulting from these factors would be very small compared with some of the uncertainties discussed below.

It has been assumed here that there are no day-night differences in the populations of the 02201 and 03301 states [*Wintersteiner et al.*, 1992]. *Lopez-Puertas et al.* [1992] have found that the day-night differences in the vibrational temperatures of these states may be as much as 8 K for some atmospheric conditions for the 02201 state and 14 K for the 03301 state in the 80- to 90-km altitude range. To test whether the increased opacity resulting from larger lower-state populations would diminish the limb radiance obtained for the group 1 bands, a set of ad hoc $2\nu_2$ vibrational temperature profiles was created with an 8 K enhancement near the mesopause, and the limb radiance was recalculated. The result is a 1% decrease in radiance in the group 1 bands at 85 km, with smaller differences for other paths. The group 2 bands are optically thin, so no change is possible due to higher $3\nu_2$ populations. Thus the effect of possible day-night differences in the populations of states 02201 and 03301 is negligible for the present study.

Lopez-Puertas et al. [1986b] (hereinafter referred to as LPb) consider a number of collisional processes which are not included here. These processes include isotope exchange of ν_3 quanta (reaction (2) from Table 2 of LPb) and the collisional relaxation processes of CO_2 (00011) on N_2, O_2, and O leading to the CO_2 (02201) state (reactions (3b), (4b), and (7b) from the same table). The primary justification for omitting these processes is that the present work treats daytime limb radiance only, where solar pumping is clearly the dominant excitation process for the 4.3-μm emitting states. Additional processes considered by LPb are expected to change the 4.3-μm radiance by very little for the sunlit case, and in the interest of simplicity they are neglected in this work.

In addition, LPb consider excitation of N_2(v=1) by OH*(v ≤ 9) (reaction (9) from Table 2 of LPb). OH, which is produced in excited vibrational states (v ≤ 9) near the mesopause by the reaction of H and O_3, may affect the 4.3-μm radiance in two ways: (1) by exchanging energy with the N_2-CO_2 reservoir through V-V transfer [*Kumer et al.*, 1978] and (2) by direct emission in the 9-8 and 8-7 bands. Since the OH production rate is small in the daytime due to the photolysis of O_3, these contributions have been neglected in the calculations reported above. Even at night it is found that the enhancements of the inband 4.3-μm limb radiance due to OH are only ~2-5 x 10^{-9} Watt cm^{-2} sr^{-1} at most, so this omission is of no consequence here.

Reactions (12)-(16) from Table 2 of LPb involve the state O_2(v=1), the population of which is considered an unknown quantity in their investigation. It is assumed here that the O_2(v=1) state is in LTE. This is certainly the case above 85 km where the V-T process with atomic oxygen dominates the behavior of O_2(v=1); thus the O_2(v=1) vibrational temperature is coupled to the kinetic temperature T. Below 45 km, everything is in LTE, including V-V processes, since collisions are so frequent. Thus it is only in the mesosphere (50- to 80-km altitude range) that O_2(v=1) may not be in LTE. We did a simple perturbation calculation of the O_2(v=1) vibrational temperature, holding other quantities fixed, and determined that it exceeds the local kinetic temperature by amounts ranging from 3.6 K to less than 1 K over this altitude range. We then calculated the additional excitation of N_2 that would occur through reaction (5) (see Table 2) if these upper bound estimates were correct and found that it is between 20 and 200 times smaller than that due to $O(^1D)$. The relaxation of the LTE restriction on the O_2(v=1) vibrational temperature could therefore enhance the CO_2(00011) vibrational temperatures, which are strongly coupled to N_2, by only a small fraction of a degree in the mesosphere. Thus the resulting limb radiance is essentially unaffected by the assumption of LTE for the O_2(v=1) state.

As pointed out by *Wintersteiner et al.* [1992], there is considerable variability in the CO_2 mixing ratio profile based on experimental information from rocket- and satellite-borne instruments (see Figure 3 of that paper). Although the vibrational temperatures calculated here are quite insensitive to the CO_2 densities [*Wintersteiner et al.*, 1990], these densities will have an appreciable effect on total limb-view radiance, especially at the higher altitudes where the limb radiance is directly proportional to CO_2 column density along the viewing path. The CO_2 mixing ratio profile used here represents an average of data reported by rocket experiments in the literature (curve D of Figure 2 of *Wintersteiner et al.* [1992]). Error bars on the experimental mixing ratio values are of the order of a factor of 2 at the higher altitudes; thus the slight underprediction of radiance values for 110-130 km seen in Figure 11 is not significant.

5. Summary and Conclusions

The RAD code calculates excited state population densities under non-LTE conditions in the atmosphere using line-by-line radiative transfer algorithms. The line-by-line algorithms have been used to calculate population densities and the corresponding vibrational temperature profiles for the important 4.3-μm emitting states of CO_2 under daytime conditions. The quenching of $O(^1D)$ by N_2 has a greater impact

on these vibrational temperatures than previously reported by other authors. Total integrated radiance in a limb view from the bands associated with each of these states has also been calculated using the NLTE code. Solar pumping is the dominant excitation process for the 4.3-μm emitting states in the daytime; the total limb radiance is not very sensitive to any other excitation processes. The largest contributors to the radiance for tangent heights in the upper mesosphere and lower thermosphere (55-95 km) are the ν_3 bands 10012-10002 and 10011-10001 (see Figure 1) where the upper states absorb sunlight at 2.7 μm and reemit preferentially at 4.3 μm. The agreement of the model calculations with SPIRE sunlit data at all altitudes, as shown in Figure 11, indicates that the model properly accounts for the important excitation processes of $CO_2(\nu_3)$ in the daytime. Thus the model has been validated by agreement with experimental results, indicating that the approach is sound. Future work will concentrate on the night and terminator models, on comparison of the model with other data sets, and on adding other processes to the model.

Acknowledgments. This work is associated with the ARC/AARC Airglow Modeling Program sponsored by the Air Force Office of Scientific Research (task 92PL005). H. Nebel acknowledges the support of the Air Force Office of Scientific Research's Summer Faculty Research Program and Research Initiation Program during the course of the work as well as support from Alfred University. P. Wintersteiner was supported under Phillips Laboratory contracts F19628-86-C-0118 and F19628-90-C-0060. We thank M. Lopez-Puertas for a number of very helpful and insightful comments and suggestions. The graphs for Figures 2-13 were generated by Armand Paboojian of ARCON Corporation.

References

Anderson, G. P., S. A. Clough, F. X. Kneizys, J. H. Chetwynd, and E. P. Shettle, AFGL atmospheric constituent profiles (0-120 km), *Rep. AFGL-TR-86-0110*, 43 pp., Air Force Geophys. Lab., Bedford, Mass., 1986.

Dickinson, R. E., Infrared radiative cooling in the mesosphere and lower thermosphere, *J. Atmos. Terr. Phys.*, *46*, 995-1008, 1984.

Gordiets, B. F., Y. N. Kulikov, M. N. Markov, and M. Y. Marov, Numerical modeling of the thermospheric heat budget, *J. Geophys. Res.*, *87*, 4504-4514, 1982.

Gueguen, H., F. Yzambart, A. Chakroun, M. Margottin-Maclou, L. Doyenette, and L. Henry, Temperature dependence of the vibration-vibration transfer rates from CO_2 and N_2O states excited in the 00^01 vibrational level to $^{14}N_2$ and $^{15}N_2$ molecules, *Chem. Phys. Lett.*, *35*, 198-201, 1975.

Harris, R. D., and G. W. Adams, Where does the $O(^1D)$ energy go?, *J. Geophys. Res.*, *88*, 4918-4928, 1983.

Hedin, A. E., MSIS 86 thermospheric model, *J. Geophys. Res.*, *92*, 4649-4662, 1987.

Inoue, G., and S. Tsuchiya, Vibration-to-vibration energy transfer of $CO_2(00^01)$ with N_2 and CO at low temperatures, *J. Phys. Soc. Jpn.*, *39*, 479-486, 1975.

James, T. C., and J. B. Kumer, Fluorescence of CO_2 near 4.3 μm: Application to daytime limb radiance calculations, *J. Geophys. Res.*, *78*, 8320-8329, 1973.

Kumer, J. B., Atmospheric CO_2 and N_2 vibrational temperatures at 40- to 140-km altitude, *J. Geophys. Res.*, *82*, 2195-2202, 1977.

Kumer, J. B., and T. C. James, $CO_2(001)$ and N_2 vibrational temperatures in the $50 \le z \le 130$ km altitude range, *J. Geophys. Res.*, *79*, 638-648, 1974.

Kumer, J. B., and T. C. James, SPIRE data evaluation and nuclear IR fluorescence processes, *Rep. DNA 6237F*, 114 pp., Def. Nucl. Agency, Washington, D. C., 1982.

Kumer, J. B., A. T. Stair, Jr., N. Wheeler, K. D. Baker, and D. J. Baker, Evidence for an $OH^* \overset{VV}{\rightleftharpoons} N_2^* \overset{VV}{\rightleftharpoons} CO_2(\nu_3) \rightarrow CO_2 + h\nu(4.3\ \mu m)$ mechanism for 4.3-μm airglow, *J. Geophys. Res.*, *83*, 4743-4747, 1978.

Kutepov, A. A., D. Kunze, D. G. Hummer, and G. B. Rybicki, The solution of radiative transfer problems in molecular bands without the LTE assumption by accelerated lambda iteration methods, *J. Quant. Spectrosc. Radiat. Transfer*, *46*, 347-365, 1991.

Lopez-Puertas, M., and F. W. Taylor, Carbon dioxide 4.3-μm emission in the Earth's atmosphere: A comparison between Nimbus 7 SAMS measurements and non-local thermodynamic equilibrium radiative-transfer calculations, *J. Geophys. Res.*, *94*, 13,045-13,068, 1989.

Lopez-Puertas, M., R. Rodrigo, A. Molina, and F. W. Taylor, A non-LTE radiative transfer model for infrared bands in the middle atmosphere. I. Theoretical basis and application to CO_2 15 μm bands., *J. Atmos. Terr. Phys.*, *48*, 729-748, 1986a.

Lopez-Puertas, M., R. Rodrigo, J. J. Lopez-Moreno, and F. W. Taylor, A non-LTE radiative transfer model for infrared bands in the middle atmosphere. II. CO_2 (2.7 and 4.3 μm) and water vapour (6.3 μm) bands and $N_2(1)$ and $O_2(1)$ vibrational levels, *J. Atmos. Terr. Phys.*, *48*, 749-764, 1986b.

Lopez-Puertas, M., M. A. Lopez-Valverde, and F. W. Taylor, Vibrational temperatures and radiative cooling of the CO_2 15 μm bands in the middle atmosphere, *Q. J. R. Meteorol. Soc.*, *118*, 499-532, 1992.

McClatchey, R. A., W. S. Benedict, S. A. Clough, D. E. Burch, R. F. Calfee, K. Fox, L. S. Rothman, and J. S. Garing, AFCRL atmospheric absorption line parameters compilation, *Rep. AFCRL-TR-73-0096*, 78 pp., Air Force Cambridge Res. Lab., Bedford, Mass., 1973.

Rosser, W. A., Jr., A. D. Wood, and E. T. Gerry, Deactivation of vibrationally excited carbon dioxide (ν_3) by collisions with carbon dioxide or with nitrogen, *J. Chem. Phys.*, *50*, 4996-5008, 1969.

Rothman, L.S., et al., The HITRAN database: 1986 edition, *Appl. Opt.*, *26*, 4058-4097, 1987.

Rothman, L. S., et al., The HITRAN molecular database: Editions of 1991 and 1992, *J. Quant. Spectrosc. Radiat. Transfer*, *48*, 469-507, 1992.

Sharma, R. D., and C. A. Brau, Energy transfer in near-resonant molecular collisions due to long-range forces with application to transfer of vibrational energy from ν_3 mode of CO_2 to N_2, *J. Chem. Phys.*, *50*, 924-930, 1969.

Sharma, R. D., and P. P. Wintersteiner, CO_2 component of daytime Earth limb emission at 2.7 μm, *J. Geophys. Res.*, *90*, 9789-9803, 1985.

Shved, G. M., G. I. Stepanova, and A. A. Kutepov, Transfer of 4.3 μm CO_2 radiation on departure from local thermodynamic equilibrium in the atmosphere of the Earth, *Izv. Acad. Sci. USSR, Atmos. Oceanic Phys., Engl. Transl.*, *14*, 589-596, 1978.

Stair, A. T., Jr., R. D. Sharma, R. M. Nadile, D. J. Baker, and W. F. Grieder, Observations of limb radiance with cryogenic spectral infrared rocket experiment, *J. Geophys. Res.*, *90*, 9763-9775, 1985.

Wintersteiner, P. P., and R. A. Joseph, Development of models for infrared emission in the upper atmosphere, *Rep. AFGL-TR-86-0163*, 91 pp., Air Force Geophys. Lab., Bedford, Mass., 1986.

Wintersteiner, P. P., and R. D. Sharma, Update of an efficient computer code (NLTE) to calculate emission and transmission of radiation through nonequilibrium atmospheres, *Rep. AFGL-TR-85-0240*, 155 pp., Air Force Geophys. Lab., Bedford, Mass., 1985.

Wintersteiner, P. P., R. H. Picard, R. D. Sharma, H. Nebel, A. J. Paboojian, J. R. Winick, and R. A. Joseph, CO_2 non-LTE effects in a line-by-line radiative excitation model, in *Technical Digest, Topical Meeting on Optical Remote Sensing of the Atmosphere, Opt. Soc. Am., 1990 Ser., vol. 4*, pp. 615-618, 1990.

Wintersteiner, P. P., R. H. Picard, R. D. Sharma, J. R. Winick, and R. A. Joseph, Line-by-line radiative excitation model for the nonequilibrium atmosphere: Application to CO_2 15-μm emission, *J. Geophys. Res.*, *97*, 18,083-18,117, 1992.

H. Nebel, Division of Physical Sciences, Alfred University, Alfred, NY 14802. (e-mail: nebel@bigvax.alfred.edu)

R. H. Picard, R. D. Sharma, J. R. Winick, Phillips Laboratory, Geophysics Directorate (OPS), Hanscom AFB, MA 01731.

P. P. Wintersteiner, ARCON Corporation, 260 Bear Hill Road, Waltham, MA 02154. (e-mail: winters@zircon.plh.af.mil)

(Received October 12, 1992; revised January 28, 1994; accepted January 28, 1994.)